Void Fraction Distribution In A Horizontal 37-Element Bundle

Uditha P.M. Senaratne And Laurence K.H. Leung

Atomic Energy of Canada Limited
Thermalhydraulics Branch, Stn 87
Chalk River Laboratories
Chalk River, ON K0J 1J0
Canada

ABSTRACT

Void fraction measurements using fibre-optic void probes in a 37-element bundle string at CANDU®[1]-equivalent operating conditions are presented. These measurements were obtained with 23 fixed probes and one traversable probe, to examine subchannel void fractions and void distributions in the bundle. The bundle-cross-sectional-average void fraction is computed using the measurements and compared against predictions of the Massena correlation and the homogeneous model.

Results show that void fraction depends strongly on the cross-sectional average thermodynamic quality. Void is initiated in inner subchannels of the bundle and spreads to intermediate subchannels with increasing power. The void distribution over the bundle cross section is relatively uniform (60% to 80% void) at high powers.

The differences between cross-sectional-average void fractions based on experimental data and those predicted using the Massena correlation are within 2% to 6% at cross-sectional-average void fractions of 10% to 40%. The differences with the homogeneous model are within 2% to 6% at cross-sectional-average void fractions exceeding 60%.

INTRODUCTION

Information on bundle cross-sectional-average void fraction and subchannel void fraction is important in the development of analytical tools for

[1] CANada Deuterium Uranium. CANDU is a registered trademark of Atomic Energy of Canada Limited.

thermalhydraulic analyses of CANDU fuel. The current approach applies tube-data-based correlations to determine the cross-sectional-average void fraction. Experimental void fraction data for bundle geometries are scarce and are associated with high uncertainty. Detailed void-fraction measurements are needed to validate these correlations. In addition, subchannel void fractions are required to validate the ASSERT subchannel code.

This paper presents results from an experiment performed at Atomic Energy of Canada Limited (AECL), Chalk River Laboratories (CRL), where the void fractions in subchannels of a 37-element bundle string were measured using fibre-optic void probes.

EXPERIMENTAL SET-UP AND TEST MATRIX

The experiment was performed in the MR-3 loop at CRL. The loop comprised two primary coolant pumps, a pre-heater, a vertical and a horizontal test station, two condensers, a vapour drum and a cooler (see Figure 1). The working fluid was Refrigerant 134-a (R-134a). Each test station has been designed to house a full-scale CANDU bundle string contained within an inner liner. The current experiment utilized the horizontal test station with an inner liner simulating an uncrept CANDU pressure tube. A dedicated, fully variable, power supply unit provided power for direct heating of the bundle string used for testing. A resistor bank that was coupled in series with the centre element and various rings of the bundle string was used to vary the radial power profile of the bundle string. The loop was fully instrumented to measure the power to the bundle string, flow through the test stations, temperatures of the elements in bundles at required locations, temperature of the working fluid and system pressure at required locations and differential pressures over segments of the test station. Data collection was via a computer-based data acquisition system (DAS).

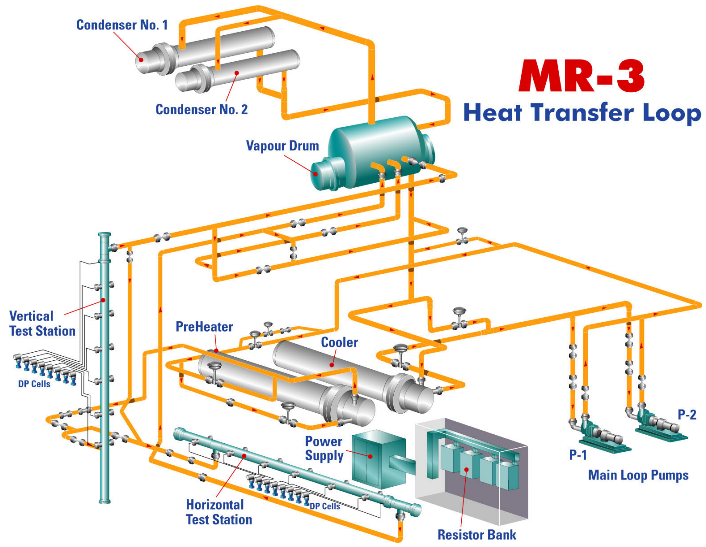

FIGURE 1: THE MR-3 LOOP

The bundle string simulated twelve aligned 37-element bundles equipped with endplates and appendages. Elements were direct-heated, hollow and fully aligned to allow for the axial traverse of thermocouple carriers. Simulated bundles were held together by machined end plates at the axial positions corresponding to bundle junctions. Hollow spool pieces, cradled in holes in the machined end plates, joined corresponding elements of adjacent bundles. The hollow spool pieces and the machined end plates simulated bundle end plugs and bundle end plates as closely as possible. Appendages (spacer and bearing pads) were also installed on elements at the appropriate axial positions.

The electrical resistance of elements generated heat in the bundle string when power was applied. The axial power profile was uniform and the radial power profile in the bundle string was achieved by varying the wall thickness of the hollow tubes to simulate the natural-uranium fuel profile. An external variable resistor bank was used to fine-tune the radial power profile to achieve that used in tests with water-cooled bundle strings.

A void probe (Figure 2) comprised of a 0.5-mm diameter Inconel tube that contained a 100-μm-diameter multi-mode silica glass fibre drawn to an exposed, tapered tip of nominal diameter 20 μm. In the present experiment, void probes were located approximately 17 mm upstream of the downstream end of the bundle string. Twenty-three fixed probes and one traversable probe were used in the experiment.

Radial locations of the 23 fixed void probes are illustrated in Figure 3. The fixed void probes were contained in one-half of the bundle formed by the vertical axis of symmetry. Elements in the other half of the bundle contained thermocouples to monitor sheath temperatures. Each instrumented subchannel contained one fixed probe at its approximate geometric centre. Two instrumented subchannels contained two additional probes each, close to their boundaries. These additional probes were used to establish the void profile within the subchannel. The traversable probe was mounted at the end of a computer-controlled, motor-driven shaft designed to move the probe along the vertical axis of symmetry in the upper half of the bundle. The probe traversed the radial distance from approximately 8 mm above the centre of the bundle (i.e., 2 mm above the top surface of the centre element) to 52 mm above the centre of the bundle (i.e., the top inner surface of the liner containing the bundle string), at an increment of 4 mm during the experiment.

At a selected set of experimental conditions, the fixed void probes provided: (a) the void profile in two subchannels of different shapes (see Figure 3), and (b) the void distribution over one-half of the cross section of the 37-element bundle about the vertical axis of symmetry. As such, void fraction data gathered using the fixed probes enabled computing the cross-sectional-average void fraction in the 37-element bundle string. The traversable probe provided the void fraction profile in the upper half of the 37-element bundle along the vertical axis of symmetry at the same experimental conditions.

Optical void probes function based on the principle that light passing through an optical fibre is totally reflected and returned when the tip of the probe is exposed to the vapour phase. Conversion of the response of the probe to an electrical signal by suitable means enables the computation of a time-average void fraction.

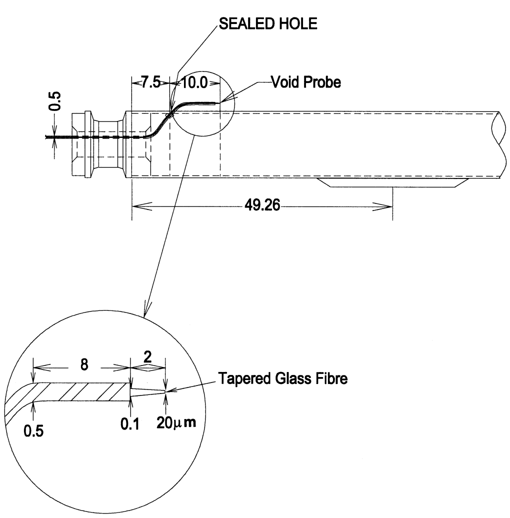

Dimensions in mm except probe tip

FIGURE 2: TYPICAL FIXED VOID PROBE

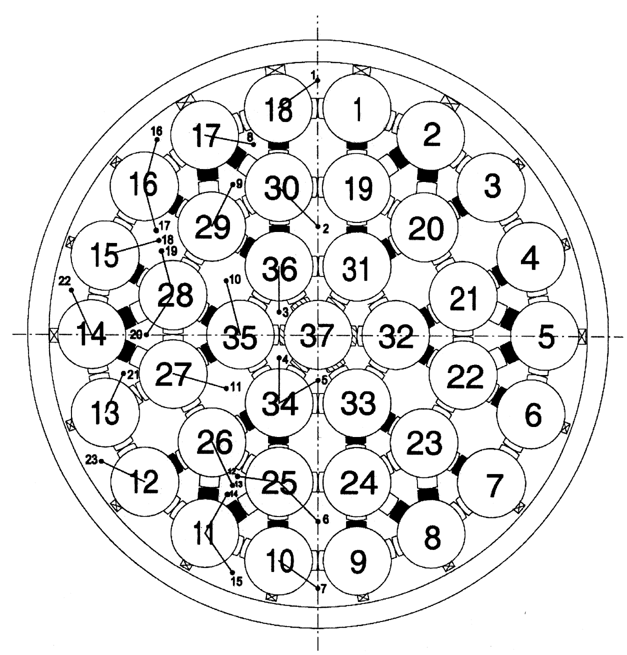

FIGURE 3: VOID PROBE LOCATIONS IN THE 37-ELEMENT BUNDLE STRING

A multi-board signal processor was used in the present experiment to read and process the responses from all void probes simultaneously over six 10-second intervals at a selected set of experimental conditions and traversable probe position, and compute a time-average void fraction. The signal processor is a technologically updated version of a unit [1] developed and used previously at CRL. The void fraction data generated in this manner were gathered by the DAS through an analog-to-digital converter and stored to disc, along with the run identification number, position of the traversable probe and loop conditions, to be retrieved later for analysis.

The void fraction measurement experiment was performed at a nominal R-134a pressure of 1.50 MPa (heavy-water-equivalent value of 9 MPa). This paper discusses data collected at nominal R-134a mass flow rates of 9.6, 12.1 and 16.0 kg/s (heavy-water-equivalent values of 14.0, 17.7 and 23.4 kg/s, respectively), R-134a inlet temperature of 39.9°C (water-equivalent value of 263.1°C) and values of power up to 80% of that required for dryout.

RESULTS AND DISCUSSION

Multiple observations of void fraction from each probe[2], with test conditions held constant and the traversable probe located at a specific radial position, were averaged. This resulted in a single value of void fraction from each probe at a selected set of experimental conditions and traversable probe location. An energy balance for each set of experimental conditions was used to calculate the cross-sectional-average thermodynamic quality at the axial location of the void probes.

Figure 4 illustrates the typical behaviour of void fraction measured using the fixed probes with cross-sectional-average thermodynamic quality at the probes at R-134a pressure (P) of 1.5 MPa, inlet temperature (T_{in}) of 39.9ºC and mass flow rate (W) of 11.8 kg/s.

[2] Data from a few probes that either had been inadvertently damaged during installation or had malfunctioned during the experiment (as indicated by the signal processing system) were removed from the database at this stage.

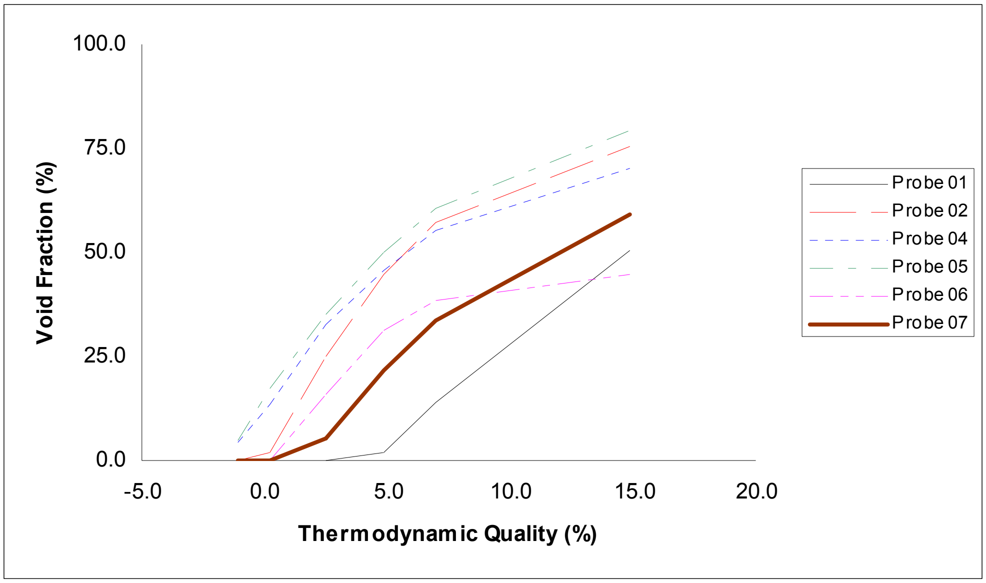

FIGURE 4: VOID FRACTION AT FIXED PROBES ALONG THE VERTICAL AXIS OF SYMMETRY

Void fraction increases as cross-sectional-average thermodynamic quality at the probes increases. In a majority of instances, void fraction approaches a maximum of 50 - 80% over the range of values of cross-sectional-average thermodynamic quality encountered in the experiment.

The rate of increase in void fraction at probes in peripheral subchannels (e.g., probe number 1 and 7) is slow at low values of cross-sectional-average thermodynamic quality (i.e., less than around 2%), and rapid at values of cross-sectional-average thermodynamic quality between 5% and 15%. In the case of probes in central subchannels (e.g., probe number 4 and 5), there is no initial region of slow increase. Void fraction increases rapidly at first up to a value of cross-sectional-average thermodynamic quality of around 15%. The rate of increase is slower at higher values of cross-sectional-average thermodynamic quality.

Void is generated at subcooled values of cross-sectional-average thermodynamic quality, especially as the coolant flow rate decreases. This is an indication of radial enthalpy imbalances within the bundle.

The behaviour of void fraction at the fixed probe locations with increasing power to the bundle string at R-134a pressure of 1.5 MPa, mass flow rate of 11.8 kg/s and inlet temperature of 39.9 ºC is shown in Figure 5. Power fraction shown in the figure signifies the power applied to the bundle string as a fraction of dryout power[3] corresponding to the flow conditions. Probe numbers are arranged by elevation in the bundle, starting at the top (see Figure 3). At a given elevation, the probes in the inner region of the bundle are indicated first.

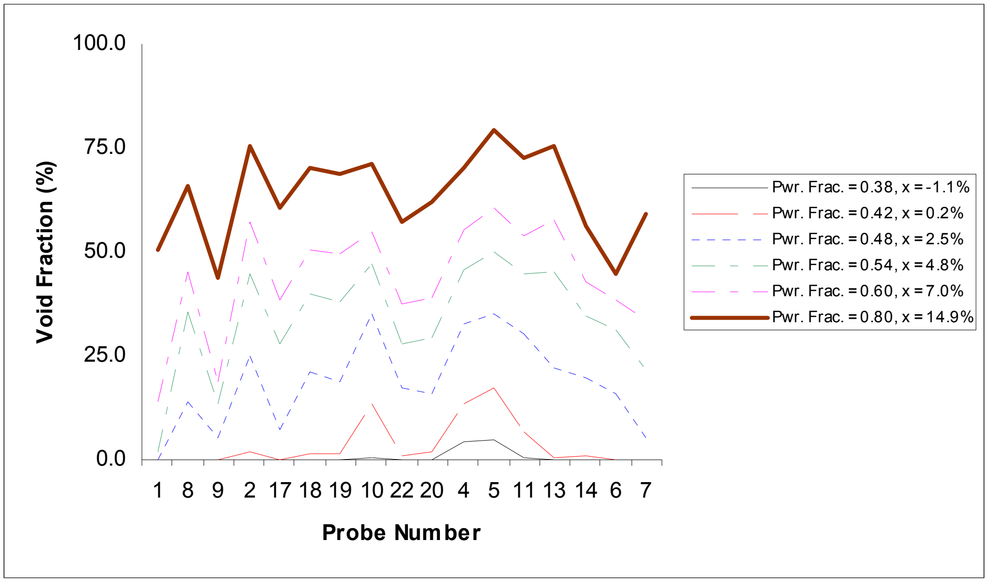

FIGURE 5: VOID FRACTION AT FIXED PROBES WITH POWER TO THE BUNDLE STRING, VOID PROBES ARRANGED BY ELEVATION

The void fraction at the fixed probe locations increases as power to the bundle string is increased. Void is initiated in the inner subchannels. (Probe number 4 and 5 are the first to indicate the presence of void at the lowest power levels.) As power is increased further, voiding spreads to the subchannels containing probe number: (a) 2, 10 and 11, (b) 13 and 14, (c) 17, 18 and 19, (d) 22, (e) 7, and (f) 1. This is determined by the magnitude of the void fraction readings at these probe locations as power is increased. The order in which void is detected in subchannels may not be exactly as above.

Readings from probe number: (a) 13 and 14, and (b) 17, 18 and 19, indicate that a void fraction profile exists within subchannels. Void fraction is higher at the centre of the subchannel when individual readings are in excess of 10%.

Void fraction increases in the inner and intermediate subchannels of the upper region of the bundle (probe number 2, 8, 10 and 17 through 19) as well as in the inner and intermediate subchannels of the lower region of the bundle (probe number 5, 11, 13 and 14) as power to the bundle is increased as a fraction of

---

[3] Dryout power for a particular set of flow conditions is the power applied to the bundle string at which a single initial dryout is detected anywhere in the bundle string at those flow conditions.

dryout power. Furthermore, the void fraction in the inner and intermediate subchannels in the lower region of the bundle is generally comparable with, or higher than that in the inner and intermediate subchannels of the upper region of the bundle. Even in the case of the upper region, the void fraction at the top of the bundle (as indicated by probe number 1) is somewhat less than that in the inner subchannels (e.g., as indicated by probe number 8 and 2). Therefore, there is no compelling indication of flow stratification at the mass flow rates used in the present experiment.

Typical uncertainties (2σ) in the data of Figure 4 and Figure 5 have been estimated to range from around 7% to 8% at low values of void fraction (i.e., less than around 10%) to around 4% to 6% at high values of void fraction (i.e., greater than 50%).

Figure 6 illustrates the typical void profile along the vertical axis of symmetry in the upper half of the bundle string, obtained using the traversable probe. As in Figure 5, power fraction signifies the power applied to the bundle string as a fraction of dryout power corresponding to the flow conditions. The pitch circle diameter (PCD) of the outer, intermediate and inner ring (i.e., the radial location of the inter-element gap) is indicated in the figure as well.

Void is first observed in the subchannel closest to the centre element, at the radial position closest to the upper surface of the centre element. Void is concentrated in the inner subchannels at values of thermodynamic quality below around 2%. Void spreads over all the monitored subchannels at values of thermodynamic quality of around 6% to 7%.

As thermodynamic quality increases to the extent where void readings are greater than around 8% to 10%, a void profile is clearly visible within all subchannels across which the traversable probe was moved. (The radial positions of the inter-element gaps, as denoted by the PCD of the inner, intermediate and outer rings, help in locating the lower and upper boundaries of subchannels along the vertical axis of symmetry in the upper half of the bundle.) Void fraction is seen to be maximum at the centre of subchannels, and minimum at the lower and upper boundaries.

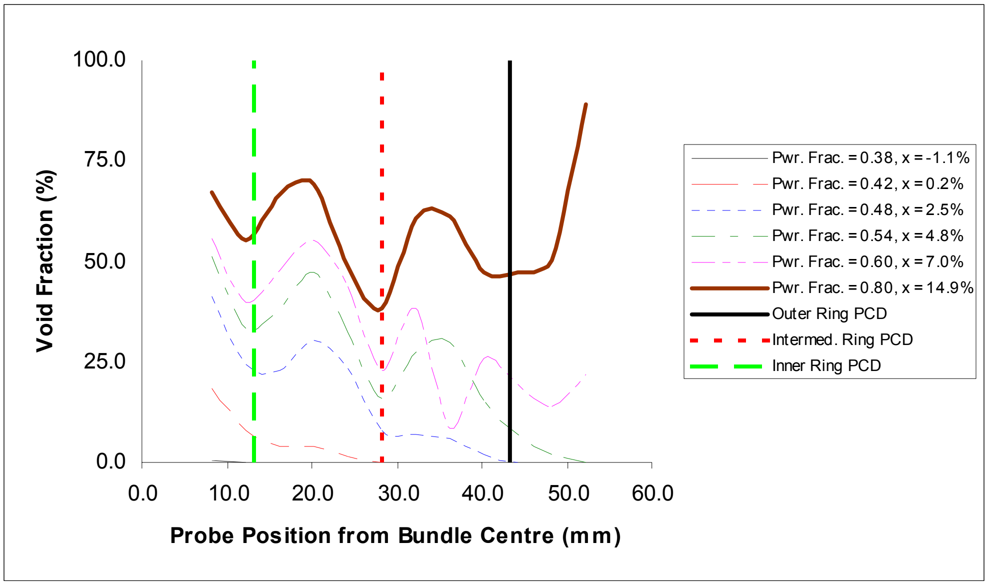

FIGURE 6:VOID FRACTION PROFILE USING THE TRAVERSABLE PROBE WITH POWER TO THE BUNDLE STRING

When the power to the bundle is sufficient for the void fraction at the centre of the monitored subchannels to be around 70% or higher (which corresponds to values of thermodynamic quality exceeding around 15%), the distribution of void in the monitored subchannels appears to be nearly identical across all the subchannels. The observed peak in void fraction at the top surface of the liner is thought to be the result of collection of vapour in a groove that was made in the liner to prevent damage to the traversable probe due to contact with the liner at the upper limit of its traverse.

Average void fraction data from fixed void probes at the centre of instrumented subchannels were corrected: (a) for instrumentation error (or bias), and (b) to account for the void profile in subchannels (since the fixed probe at the centre of a subchannel generally indicates a reading that is higher than the subchannel-average void fraction). The resulting data were used to compute values of cross-sectional-average void fraction, using the cross-sectional area of subchannels as the weighting factor. Results were compared with the void fraction predicted using: (a) the Massena correlation [2], and, (b) the homogeneous model.

Figure 7 shows the behaviour of: (a) cross-sectional-average void fraction, and (b) void fraction predicted using the Massena correlation [2] and the homogeneous model, with cross-sectional-average thermodynamic quality. The presence of void is indicated at subcooled values of cross-sectional-average thermodynamic quality. The rate of increase in cross-sectional-average void fraction is: (a) slow at subcooled values of cross-sectional-average thermodynamic quality, (b) rapid up to values of cross-sectional-average thermodynamic quality of around 10%, and (c) slow again when the cross-sectional-average thermodynamic quality exceeds 10%.

At subcooled values of thermodynamic quality, the values of cross-sectional-average void fraction based on experimental data are indicated to be somewhat larger than the void fraction predicted using the Massena correlation [2] and the homogeneous model. However, the uncertainty of experimental data used in calculating the cross-sectional-average void fraction in this region is large relative to the deviations.

At values of thermodynamic quality between approximately 2% and 7%, values of cross-sectional-average void fraction based on experimental data are: (a) less than those predicted by the homogeneous model, and (b) generally closer to values predicted using the Massena correlation [2].

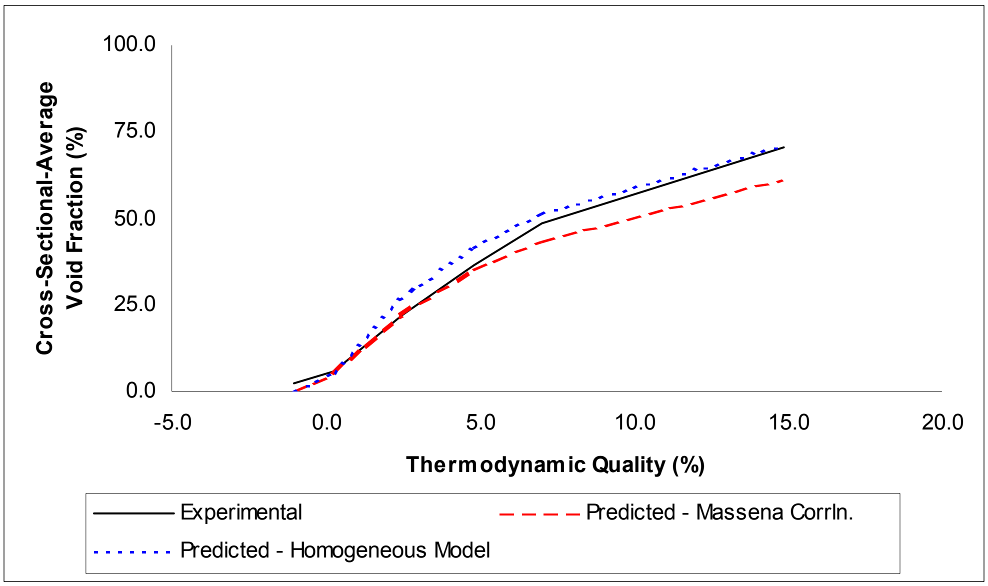

P = 1.5 MPa, T_{in} = 39.9°C, W = 11.8 kg/s

FIGURE 7: EXPERIMENTAL AND PREDICTED CROSS-SECTIONAL-AVERAGE VOID FRACTION

At values of thermodynamic quality exceeding 10%, values of cross-sectional-average void fraction based on experimental data are: (a) greater than those predicted using the Massena correlation [2], and (b) generally closer to values predicted by the homogeneous model.

CONCLUSIONS

1. Cross-sectional-average and subchannel void fraction are significantly influenced by thermodynamic quality. The rate of increase of cross-sectional-average void fraction is gradual with thermodynamic quality at subcooled conditions, relatively rapid at thermodynamic qualities between 2% and 10%, and becomes gradual again at higher qualities.
2. A void fraction profile exists in subchannels, as indicated by the readings from the traversable void probe. A majority of readings show that the void fraction at the centre of a subchannel is largest in magnitude.
3. Void is initiated in the inner subchannels (as indicated by the traversable probe when positioned close to the centre element and the fixed probes in the inner subchannels). Void spreads to the intermediate and outer subchannels as power to the bundle string is increased.
4. The traversable probe indicates that void fraction in intermediate subchannels is larger at intermediate values of power to the bundle string. At high values of power to the bundle string (i.e., at values of void fraction exceeding around 60%), there is little variation in the value of void fraction in all subchannels that were monitored. A majority of void fraction readings are in the range 60% – 80%. The variation in void fraction readings is much more significant at low power.
5. Cross-sectional-average void fraction can be predicted reasonably well using the Massena [2] correlation at values of thermodynamic quality between approximately 2% and 7%. The homogeneous model is seen to predict the cross-sectional-average void fraction quite well at values of thermodynamic quality exceeding 10%.
6. The void fraction database offers a unique opportunity to assess system and subchannel codes used in thermalhydraulic analyses of nuclear reactors.

ACKNOWLEDGEMENTS

The authors gratefully acknowledge the financial support of the CANDU Owners' Group (COG), which facilitated this experimental study.

REFERENCES

[1] NICKERSON, J.R., COWHEY, R.J. and MCKENNA, J.A., "An Electronics Package for Local Void Fraction Measurement Using Hot Film, Conductance

and Fibre Optic Probes", Third AIAA / ASME Joint Thermophysics, Fluids and Heat Transfer Conference, St, Louis, MO, pp 103 – 107, 1982

[2] MASSENA, W.A., "Steam Water Pressure Drop and Critical Discharge Flow – A Digital Computer Program", General Electric, Hartford Atomic Products Operation, Report HW-65706, Richland, Washington, June 1960